PCCP

Accepted Manuscript

ROYAL SOCIETY OF CHEMISTRY

www.rsc.org/pccp

Theoretical Study in Interactions Fluorinated Organomercurials with Arene and Gold Fragments

Fernando Mendizabal*[ab], Sebastián Miranda-Rojas*[c] and Lorena Barrientos-Poblete[de]

[a]Departamento de Química, Facultad de Ciencias, Universidad de Chile, P.O. Box 653, Las Palmeras 3425, Ñuñoa, Santiago, Chile.

[b]Millennium Nucleus of "Molecular Engineering for Catalysis and Biosensors", ICM, Chile.

[c]Núcleo Milenio "Chemical Processes and Catalysis" (CPC), Departamento de Ciencias Químicas, Facultad de Ciencias Exactas, Universidad Andres Bello, Avenida República 275, Santiago, Chile.

[d]Departamento de Química, Facultad de Ciencias Básicas, Universidad Metropolitana de Ciencias de la Educación, Casilla 147, Santiago, Chile.

[e]Center for the Development of Nanoscience and Nanotechnology, CEDENNA, Santiago, Chile

Abstract

The electronic structure and spectroscopic properties of $[Hg(C_6F_5)_2]_2$-{L}, $[Hg_3(o\text{-}C_6F_4)_3]_2$·{L} (L = naphthalene, biphenyl, fluorene) and $[Hg_3(o\text{-}C_6F_4)_3]\{Au_3(\mu\text{-}C(OEt)=NC_6H_4CH_3)_3\}_n$ (n = 1,2) adducts were studied at the HF, MP2, SCS-MP2, DFT and DFT-D3 levels. The intermolecular interactions among the fragments were analyzed using the levels of calculation proposed. The energy decomposition analysis at the TPSS-D3 level was used to define the dominant components of the interaction. The van der Waals interactions between mercury and arene (Hg-arene) were found to be the main short-range stability contribution in the $[Hg(C_6F_5)_2]_2$-{L} and $[Hg_3(o\text{-}C_6F_4)_3]_2$·{L} complexes. At the MP2, SCS-MP2 and DFT-D3 levels, equilibrium Hg-C distances are between 360 and 310 pm. The pair-wise energies were found between 18.0 and 6.0 kJ/mol. In the $[Hg_3(O\text{-}C_6F_4)_3]\{Au_3(\mu\text{-}C(OEt)=NC_6H_4CH_3)_3\}_n$ (n = 1,2) complexes the

metallophlic intermolecular interaction Hg---Au. Pair-wise energies of 85.7, 39.4, 78.1 and 57.9 kJ/mol were found at the MP2, SCS-MP2, TPSS-D3 and PBE-D3 levels with the $[Hg_3(o\text{-}C_6F_4)_3]\{Au_3(\mu\text{-}C(OEt)=NC_6H_4CH_3)_3\}$ model. The same trend is maintained for $[Hg_3(o\text{-}C_6F_4)_3]\{Au_3(\mu\text{-}C(OEt)=NC_6H_4CH_3)_3\}_2$ model: 73.4, 29.3, 70.6 and 61.3 kJ/mol by MP2, SCS-MP2, TPSS-D3 and PBE-D3, respectively. The absorption spectra of these complexes were calculated by the single excitation time-dependent method at the TPSS-D3 level to validate out models against the experimental data.

I. Introduction

The supramolecular chemistry of trimeric perfluoro-ortho-phenylenemercury [$Hg_3(o\text{-}C_6F_4)_3$] and bis(pentafluorophenyl)mercury [$Hg(C_6F_5)_2$] forming adducts with a variety of arenes (benzene, biphenyl, naphthalene, fluorene, etc.), aldehydes, ketones, amides, nitriles, phosphoramides, and sulfoxides has been widely investigated.[1-13] Furthermore, [$Hg_3(o\text{-}C_6F_4)_3$] forms a complex with {$Au_3(\mu\text{-}C(OEt)=NC_6H_4CH_3)_3$}, dominated by intermolecular interactions of the Hg^{II}-Au^{I} (d^{10}-d^{10}) metallophilic type.[14,15] Perfluorinated aromatic mercury molecules show strong Lewis acidity, while arenes and {$Au_3(\mu\text{-}C(OEt)=NC_6H_4CH_3)_3$} molecules act as Lewis bases. These classes of compounds have been reported to form adducts with interesting coordination chemistry. In general, the donor-acceptor interaction invokes dispersion and electrostatic intermolecular forces that probably add to the stability of the adducts.[16-18] The above description is within the area which is called supramolecular chemistry.[19-21]

The intermolecular term is a synonym of non-covalent, which is explained by interactions of the electrostatic, hydrogen bonding and van der Waals type.[22,23] The expression "non-covalent" implies that the association type between two or more molecules is not explained by the traditional chemical bond concept, e.g. sigma bond with two electrons. Non-covalent intermolecular interactions are characterized by acting over long distances, between 200 pm and 400 pm. Thus, orbital overlapping is not necessary.[24] The attraction between the subsystems is due to the electrical properties of the molecules that are associated. The corresponding energy terms are called electrostatic, inductive, and dispersion.[25,26] The total stabilization energy when molecules associate themselves to form a supramolecular structure is between 1 and 100 kJ/mol, considerably less than a covalent bond energy (400 kJ/mol).[22,23] Thus, the description

and study of non-covalent interactions requires very precise methods of quantum chemistry that include the correlation and dispersion energies.

The understanding of compounds comes from the observation of structures and patterns, coupled with the theory and calculation of the intermolecular interaction energies.[27,28] Data on molecular structures and their interactions come from their crystalline phase. In general, when there are two or more very heavy atoms (gold, thallium, mercury, etc.) in the studied complexes, they show evidence of metallophilic interactions.[29,30] At the theoretical level, the metallophilic attraction is estimated when electronic correlation effects are taken into account, strengthened by relativistic effects.[31,32] In this respect, our goal is to advance in the understanding of the supramolecular interactions in $[Hg_3(o\text{-}C_6F_4)_3]$-{arenes}, $[Hg(C_6F_5)_2]$-{arenes} (biphenyl, naphthalene, fluorene) and $[Hg_3(o\text{-}C_6F_4)_3]\{Au_3(\mu\text{-}C(OEt)=NC_6H_4CH_3)_3\}$ systems, which imply that the type of partnership that is established between two or more molecules is explained by traditional chemical bonding.

From the theoretical point of view, density functional theory (DFT) studies of the $[Hg_3(o\text{-}C_6F_4)_3]$ complex indicate that the LUMO spans the three mercury centers (6p) and forms a large lobe that protrudes above and below the molecular plane.[33] The result suggests that this particular region of the molecule is where Lewis acidity (acceptor) is at a maximum. In agreement with that, this large lobe appears directly aligned with the direction along which Lewis base substrates approach the molecule.[33] Also, the electronic structure and spectroscopic properties of $[Hg_3(o\text{-}C_6F_4)_3]_n\cdot$\{benzene\} (n = 1,2) have been studied at the HF, MP2 and PBE levels.[18] The interaction between $[Hg_3(o\text{-}C_6F_4)_3]$ and benzene at the HF and MP2 levels was analyzed. The van der Waals

interactions (Hg-benzene) were found to be the main short-range stability contribution in the $[Hg_3(o\text{-}C_6F_4)_3]\cdot\{benzene\}$ complex. At the MP2 and PBE levels equilibrium Hg-C distances of 338.4 and 361.4 pm; and interaction energies of 46.6 and 29.2 kJ/mol were found, respectively.

In this context, a theoretical study is proposed for a set of systems which show interactions among acid-base centers like $[Hg_3(o\text{-}C_6F_4)_3]$-{L}, $[Hg(C_6F_5)_2]$-{L} (L = naphthalene, fluorene, biphenyl)[6-8] and $[Hg_3(o\text{-}C_6F_4)_3]\{Au_3(\mu\text{-}C(OEt)=NC_6H_4CH_3)_3\}$.[14,15] Theoretical models based on quantum chemistry calculations at the MP2 and DFT with dispersion levels are used.

II. Models and Computational Methods

The $[Hg(C_6F_5)_2]_2$-{L} (**1-3**), $[Hg_3(o\text{-}C_6F_4)_3]_2$-{L} (**4-6**) (L = naphthalene, fluorene, biphenyl) and $[Hg_3(o\text{-}C_6F_4)_3]\{Au_3(\mu\text{-}C(OEt)=NC_6H_4CH_3)_3\}_n$ (**7-8**) (n =1,2) models used in our study are depicted in schemes 1 and 2. C_1 symmetry has been used in all models. The geometries were fully optimized at the scalar quasirelativistic HF, MP2, SCS-MP2, PBE, TPSS and B97 levels in the gas phase. Also, in the DFT functionals PBE, TPSS and B97, Grimme dispersion correction was used for those functionals for which it is available, and its use is indicated by appending “DFT-D3” to the acronym of the density functional.[34-36] Although it is known that the MP2 approximation exaggerates such attractive interactions, it gives a good indication of their existence.[29-32] A more precise post-Hertee-Fock level is CCSD(T), although recently calculations with the spin-component-scaled (SCS) MP2 method have produced results comparable to CCSD(T) at a lower computational cost.[37-39] Thus, SCS-MP2 is considered as an accurate and efficient tool for incorporating electronic correlation to the study of large systems with a

low computational cost.[40] As Professor Pekka Pyykkö said: "thus justifying SCS-MP2 as ´poor man´s CCSD(T)´.[39]

Single point calculations of these geometries were simulated to study the excitation spectra with DFT with the time-dependent (TD-DFT) at the TPSS-D3 level,[41,42] which is based on the random-phase approximation (RPA) method[42]. The TD-DFT calculations do not evaluate the spin-orbit splitting and the values are averaged. All simulation absorption spectra have been obtained in gas phase.

The calculations were done using the Turbomole package (version 6.6).[43] For Au and Hg, the 19 valence-electron (VE) and 20 VE scalar quasirelativistic Stuttgart pseudopotentials (PP) of Andrae et al.[44] were employed, respectively. We used two *f*-type polarization functions on gold (α_f = 0.20,1.19)[31] and mercury (α_f = 0.50, 1.50).[45] Also, the augmented correlation-consistent valence-triple-zeta (aug-cc-pVTZ) basis sets were used for C, N, O, F and H. For MP2 and DFT levels, the efficient resolution of identity (RI) approximation was used to obtain the final geometry and make the calculation feasible.[46]

The energy decomposition analysis was carried out by using the Morokuma-Ziegler scheme as implemented in ADF.[47] This approach allows partitioning the interaction energy into three major energy contributions: the stabilization due to orbital mixing (ΔE_{orb}), the quasiclassical electrostatic contribution from the interaction between the frozen charge densities of the two fragments (ΔE_{elstat}), and the destabilizing term from the interaction between electrons of the same spin, or Pauli exchange (ΔE_{pauli}). Normally, the ΔE_{elstat} and ΔE_{pauli} contributions are grouped into one term defined as ΔE_{steric} (ΔE_{elstat} + ΔE_{pauli}). All ADF calculations were performed by using the TPSS

density functional with the TZP basis set. Finally, the dispersion contribution to the total interaction energy was considered as an additional fourth term and it was calculated according to the approach presented by Grimme.[34-36]

Finally, in order to obtain more insights concerning the nature of the intermolecular interactions between the ligands, we used the non-covalent interactions (NCIs) analysis.[48,49] This is an index that allows to detect and identify in real space the attractive or repulsive interactions, indicated by the regions where the reduced density gradient (RDG) reaches values near zero in the low-density region between the monomers. The NCI analysis allows to generate color-coded isosurfaces that represent these interactions in the intermolecular space in a chemically intuitive manner. The regions of the surface colored in blue represents the strong-attractive interactions (e.g. hydrogen bonds), in green are the weak-attractive interactions (e.g. van der Waals interactions), in yellow are the weak-repulsive interactions and in red are the strong-repulsive interactions. The analysis was performed from the output densities obtained at the TPSS-3D level.

III Results and Discussion

A. Molecular Geometries and Non-covalent Interaction Energies

$[Hg(C_6F_5)_2]_2$-{L} (1-3). We have fully optimized the geometries for models **1-3**. Table 1 summarize the main structural and energetic parameters, in addition to relevant structural experimental data.[6-8] The geometries obtained for the $[Hg(C_6F_5)_2]_2$-{L} (L = naphthalene, fluorene, biphenyl) complexes at the HF, MP2, SCS-MP2, DFT and DFT-D3 levels are in good agreement with the experimental data. It is seen that the structural

parameters change from the HF and DFT to the MP2, SCS-MP2 and DFT-D3 levels in all models (**1-3)**. Regardless of the method used, the intramolecular geometric parameters are very close to the experimental. We have defined as our geometric reference the intermolecular average distance between mercury and the carbons from the aromatic ring closest to the metal (Hg-C(arene)).

In all models, the usual correlation-induced shortening of the interaction distance is found for the geometries obtained with MP2, SCS-MP2 and DFT-D3 calculations. The comparison between MP2 and experimental distances showed a shortening of the MP2 Hg-C(arene) distances for biphenyl and fluorene with respect to the experimental values (see Table 1). Nevertheless, the effect of electronic correlation (MP2) and dispersion (D3) certainly improved our results. This is evidenced in the ability of these methods to provide geometries closer to the experimentally determined than the obtained with the methods without the dispersion contribution. These results suggest that the complexes involve van der Waals interactions between mercury and arene (Hg-arene), exposed by the shortening of the Hg-C(arenes) distances when using MP2 and DFT-D3 methods. At SCS-MP2-level results show an expected behavior, the distances are closest to the experimental. On the other hand, HF and DFT levels show longer Hg-C(arene) distances. This shows that when using methods that do not include dispersion effects, the attraction between $[Hg(C_6F_5)_2]_2$ and arenes decreases, thus being unable to reproduce the experimental results.

The conformational binding mode and the NCI analysis of the $[Hg(C_6F_5)_2]_2$-{L} (L = naphthalene, fluorene, biphenyl) complexes are presented in Figure 1. The binding mode of naphthalene is characterized by two types of non-convalent interactions. The first involves one of the aromatic rings of the naphthalene located between two of the

pentafluorinated rings from $[Hg(C_6F_5)_2]_2$, forming a sandwich type conformation through π-stacking interactions. An interesting feature of this attractive interaction is the direct participation of the fluoride atoms, revealed by the green surface located between the fluorides and the naphthalene. For the second interaction, each Hg^{II} is located on top of one of the carbon atoms from the second aromatic ring as illustrated in Figure 1, interactions of attractive nature. For the case of fluorene, the sandwich conformation is formed between the two perfluorinated rings and the indene moiety from fluorene. The NCI representation shows that the contribution of the fluorine atoms to the interaction with fluorene is more marked than with naphthalene. These results also highlight the role of this particular halogen on the stabilization of the complexes. The two Hg^{II} cations interact with opposite sides of the second six membered ring in a sort of cation-π-cation interaction, where both metals are located near the center of the ring. The attractive nature of this interaction is denoted by the green surface located above the carbon atoms from the fluorene ring. Regarding biphenyl, it followed a similar pattern of interaction with respect to the other two ligands. However, the two perfluorinated rings that are not interacting with biphenyl suffered a strong packing, as showed in Figure 1C. This interaction shortened the Hg-C(arene) interaction distances as evidenced from the data in Table 1. While the attractive components to the interaction seemed to be larger, there are also more repulsive contributions that may avoid the stabilization of the complex due to steric-electronic clashes. These are due to the close proximity between the rings as pointed out by the red regions of the surface.

We have estimated the intermolecular interaction $[Hg(C_6F_5)_2]_2$-{L} energies for models **1-3** with counterpoise correction (CP) for the basis-set superposition error

(BSSE). The results listed in Table 1 expose an attractive interaction between mercury and arene fragments. This interaction is more pronounced at the MP2, SCS-MP2 and DFT-D3 than HF and DFT levels, where the latter methods showed very low interaction energy. The energy minimum would still be associated with electrostatic and induction contributions. We obtained shorter Hg-C(arene) equilibrium distances, with values of 339.5, 347.8 and 350.8 pm at the MP2 level with interaction energies of 214.4, 213.4 and 251.7 kJ/mol for naphthalene, biphenyl, and fluorene, respectively. At the SCS-MP2, the interaction energies in the same complexes are -122.5, -111.2 and -125.4 KJ/mol naphthalene, biphenyl, and fluorene, respectively. When the interaction energies are featured between MP2 and SCS-MP2, It is possible to appreciate the decrease of magnitude calculated when passing to the SCS-MP2 level. The results at the DFT-D3 levels showed a similar trend, with slightly longer Hg-C(arene) distances and lower interaction energies.

The van der Waals interactions between mercury and arene (Hg-arene) were associated to the differences in energy and Hg-C(arene) distance between the MP2/DFT-D3 and HF/DFT methods at the equilibrium geometry described in Table 1. If the equilibrium geometry complex energy, $V(R_e)$, is divided by the number of closest Hg-C(arene) contacts present in the naphthalene complex, pair-wise energies of 17.8, 8.8, 8.2 and 5.9 kJ/mol are found at the MP2, PBE-D3, TPSS-D3 and B97-D3 levels, respectively. The same pattern is repeated for systems with biphenyl and fluorene. We have found that the interaction energy is mainly due to an electronic correlation effect. The difference between the MP2 and DFT-D3 methods is due to the treatment of the electronic correlation.

$[Hg_3(o\text{-}C_6F_4)_3]_2$-L (4-6). We have fully optimized the geometries for models **4-6** $[Hg_3(o\text{-}C_6F_4)_3]_2\cdot\{L\}$ L = naphthalene, fluorene, biphenyl). Table 2 shows the main geometric parameters, together with relevant experimental structural data and interaction energies. The theoretical results are in agreement with the experimental data when the $[Hg_3(o\text{-}C_6F_4)_3]\cdot\{L\}$ complexes are compared at the HF, MP2, SCS-MP2, DFT and DFT-D3 levels. Table 2 shows that the structural parameters change from the HF and DFT to the MP2 and DFT-D3 levels in all the models (**4-6)**. The intramolecular geometric parameters are close to the experimental. Following the same trend that was found for the $[Hg(C_6F_5)_2]_2$-{L} complexes, the usual correlation-induced shortening is found for MP2, SCS-MP2 and DFT-D3 calculations, suggesting intermolecular attractions among mercury and C(arene) atoms. The Hg-C(arene) distances show a van der Waals attraction which is shorter than the experimental values at the MP2, SCS-MP2 and DFT-D3 levels. As mentioned above, the MP2 approximation overestimates the van der Waals interactions,[11] while SCS-MP2 and DFT-D3 generates intermediate results very close to the experimental. On the other hand, HF and DFT describe longer Hg—Hg and Hg-C distances. The effect of dispersion is clearly demonstrated here.

The binding modes between $[Hg_3(o\text{-}C_6F_4)_3]_2\cdot$and the arene ligands showed in Figure 2, did not involve a sandwich type conformation. Instead, the benzene and indene moieties from naphthalene and fluorene (Figure 2A and 2B), respectively; interacted with only one perfluorinated ring. The other side on the aromatic moiety from the ligands interacted with a Hg^{II} from the opposite $Hg_3(o\text{-}C_6F_4)_3$ layer. The second aromatic ring from naphthalene tends to locate between two Hg^{II} atoms from opposite layers, in a similar conformation as the observed with $[Hg(C_6F_5)_2]_2$. The NCI analysis reveals that the naphthalene mainly interacts with the $Hg_3(o\text{-}C_6F_4)_3$ layer with which it was able to

establish the interaction with the $3Hg^{II}$ core, instead of preferring the π-stacking interaction with the other layer. Meanwhile, the second six membered ring from fluorene interacts with the $3Hg^{II}$ core from both layers, even though it seems to interact more closely with one layer. The nature of the interaction was exposed by the green surface that represents the attractive interaction present between the Hg^{II} atoms and the fluorene ligand. Apparently, the π-stacking interaction does not contribute significantly to the stabilization of the complex. Regarding biphenyl (Figure 2C), one of its rings partly interacts with two perfluorinated rings in a sort of pararell-displaced π-stacking interaction. The second ring of biphenyl interacts with the center of the $3Hg^{II}$ core from both layers. The NCI analysis showed a clear preference for one layer, where one of the benzene moieties closely interacts with the $3Hg^{II}$ core.

We have estimated the intermolecular $[Hg_3(o\text{-}C_6F_4)_3]$-{L} equilibrium geometry complex energies, $V(R_e)$, for models **4-6** with counterpoise correction (see Table 2). Models **4-6** produced an attraction at the MP2 and DFT-D3 levels. At the MP2 level we get the following interaction energies: 115.1, 110.5 and 143.8 kJ/mol for naphthalene, biphenyl, and fluorene, respectively. These are smaller magnitudes than those obtained in the $[Hg(C_6F_5)_2]_2$-{L} systems at the same level as the MP2 calculation. As with the previous models **1-3**, at the SCS-MP2 level results show interaction energies lower: 98.4, 96.5 and 132.1 for naphthalene, biphenyl, and fluorene, respectively. The results at the DFT-D3 levels show a similar trend. When we go to the HF and DFT levels, we can see that there is no evident minimum, or if there is it is very low.

We associate the van der Waals interactions Hg_3-C(arene) as the MP2, SCS-MP2 and DFT-D3 energies at the equilibrium distances. When the equilibrium geometry

complex energy, $V(R_e)$, is divided by the number of closest Hg-C(arene) contacts present in models (**4-6**), pair-wise energies of 9.6, 9.2 and 11.9 kJ/mol are found at the MP2 levels for naphthalene, biphenyl, and fluorene, respectively. The same trend is maintained for methods at the DFT-D3 levels studied here. We have found that the interaction energy is mainly due to an electronic correlation effect. From a theoretical standpoint, in literature there are reports on the $[Hg_3(o\text{-}C_6F_4)_3]_n$·{benzene} models (n = 1,2), where Hg-C(benzene) pair-wise interaction energy estimated at 7.8 kJ/mol is found at the MP2 level.[18] This result is very close to those proposed for the **4-6** adducts.

$[Hg_3(o\text{-}C_6F_4)_3]\{Au_3(\mu\text{-}C(OEt)=NC_6H_4CH_3)_3\}_n$ (7-8). The optimized geometries are given in Table 3. We can see that the intramolecular geometric parameters in the $[Hg_3(o\text{-}C_6F_4)_3]$ and $\{Au_3(\mu\text{-}C(OEt)=NC_6H_4CH_3)_3\}_n$ clusters are very similar regardless of the method used. On the contrary, the Hg^{II}--Au^{I} (d^{10}-d^{10}) intermolecular distances between the fragments in models **7-8** showed differences depending on the proposed methods. In order to compare and systematize the metallophilic intermolecular interaction, we have included the previously reported $V(R_e)$ in Table 3. For comparison, we also included data from experimental structures.[14] At the MP2, SCS-MP2, PBE-D3 and TPSS-D3 levels, the Hg^{II}--Au^{I} intermolecular distances are shorter and comparable to the experimental result in both models. In particular, MP2, SCS-MP2 and TPSS-D3 levels have very close results, while PBE-D3 Hg^{II}--Au^{I} distance was longer. This same trend is observed in the intermolecular interaction energy: MP2 ~ TPSS-D3 > PBE-D3> SCS-MP2.

When the $V(R_e)$ in models **7** and **8** at the MP2, SCS-MP2 and DFT-D3 levels at the equilibrium distances are divided by the number of closest Au(I)-Hg(II) contacts present, pair-wise energies of 85.7, 39.4, 78.1 and 57.9 kJ/mol are found at the MP2, SCS-MP2, TPSS-D3 and PBE-D3 levels for model **7**. The same trend is maintained for

model **8**: 73.4, 29.3, 70.6 and 61.3 kJ/mol at the MP2, SCS-MP2, TPSS-D3 and PBE-D3, respectively. In both models (**7** and **8**) we can see that the interaction energies decrease when the SCS-MP2 method is invoked. These results are obtained by subtracting, at the equilibrium distance, the energies at the HF, TPSS and PBE levels, respectively. The electronic correlation effect is the main contribution in the intermolecular interaction in both models. From a theoretical standpoint, the $[Hg(C_6F_5)_2]$---$[Au(C_6F_5)(PH_3)]$ model is reported in the literature, where an Hg^{II}--Au^{I} contact interaction of 77.3 kJ/mol has been estimated at the MP2 level.[50,51] This result is within the magnitude found by us in the models studied.

For the second group of results, the HF and DFT levels showed strong and large oscillations in the Hg^{II}--Au^{I} distance. These methods do not contain electronic correlation and dispersion effects, so they are unable to describe the Hg^{II}--Au^{I} metallophilic interactions in models **7** and **8**.

B. Energy Decomposition Analysis

The analysis of the contributions to the interaction energies was carried out according to those obtained at the TPSS-D3 level, as in general these showed the best behavior when compared to the MP2 results. The results are listed in Table 4. Notice that the interaction energies from Table 4 do not include the energy contribution associated to the distortion from the equilibrium geometry of the isolated fragments necessary for complex formation (defined as ΔE_{prep}). It is obtained by using the fragments with the geometries adopted in the complex. However, the $V(R_e)$ term from Tables 1-3 incorporate this contribution. To corroborate that the interaction energies obtained with the methodology used in ADF are of the same order of magnitude than the

energies obtained with Turbomole, we present in Table 4 the interaction energies calculated with both programs. The results were very close in magnitude. We have attributed the small differ between both programs have used different classes of basis sets. In Turbomole have been used pseudopotentials, while that in ADF have been used TPZ basis set.

The total interaction energies for the $[Hg(C_6F_5)_2]_2$-{L} complexes in increasing order were of -83.5, -104.1 and -123.1 kJ/mol for naphthalene, biphenyl and fluorene; respectively. The comparison between naphthalene and fluorene provide insights into the role of the increase of the size of the π-system. While the electrostatic attraction for $[Hg(C_6F_5)_2]_2$-fluorene was higher than the obtained for $[Hg(C_6F_5)_2]_2$-naphthalene, the same was observed for the Pauli repulsion. These two components are directly related to the larger π-cloud of fluorene. The outcome from these two contributions resulted in a more repulsive contribution for $[Hg(C_6F_5)_2]_2$-fluorene complex, denoted by the higher steric contribution than the obtained with naphthalene. Then, it is suggested that the steric effect seems to be disfavored by the size of the π-cloud, which is only slightly compensated by a larger orbital stabilization present when using fluorene. The dominant contribution responsible of the attractive nature of the interaction and the ca. 40 kJ/mol of difference between naphthalene and fluorene are the dispersion forces, which are able to overcompensate the repulsive steric effect.

The interaction energy between $[Hg(C_6F_5)_2]_2$ and the biphenyl ligand needs to be analyzed separately, because as described above, it showed a completely different conformation than the other two ligands. The intense packing between the $[Hg(C_6F_5)_2]_2$ and the biphenyl ligand resulted in higher orbital, electrostatic and dispersion

contributions to the stabilization of the complex than the calculated for the other two ligands. However, this packing also induced a very large Pauli repulsion that decreased the interaction energy to a magnitude lower than the obtained for fluorene. Similarly to naphthalene and fluorene, the dispersion contribution overcompensate the repulsive contribution to the interaction energy.

The interaction energies for the $[Hg_3(o\text{-}C_6F_4)_3]_2 \cdot \{L\}$ complexes in increasing order were -128.2, -148.0 and -161.3 kJ/mol for naphthalene, biphenyl and fluorene, respectively. While the orbital contribution is very similar among the complexes, the steric repulsion is higher for the fluorene ligand because of the larger π-cloud with respect to the other two ligands. In this case it is more evident that the dispersion forces play a crucial role in the stabilization of these complexes, as the interaction energy is very close to the magnitude of the dispersion contribution.

The slightly lower interaction energy of naphthalene compared to biphenyl and fluorene seems to be related to the need of a certain distance between the two aromatic rings to properly interact with the perfluorinated rings and the Hg^{II} atoms simultaneously. The biphenyl fulfill this requirement through the presence of the single bond between the aromatic rings, while fluorene has a five membered ring between the two six membered rings involved in the interaction.

The interaction energy analysis shed light into the advantages of using $[Hg_3(o\text{-}C_6F_4)_3]_2$ over $[Hg(o\text{-}C_6F_5)_2]_2$. The three ligands showed an increase of ca. 40 kJ/mol in the interaction energies when moving from $[Hg(o\text{-}C_6F_5)_2]_2$ to $[Hg_3(o\text{-}C_6F_4)_3]_2$. Interestingly, each ligand interacts with only one of the three perfluorinated rings, pointing out that the increase in the number of Hg^{II} atoms entails the increase of the

interaction strength. For the particular cases of naphthalene and fluorene it is mainly due to an increase of the dispersion contribution, whereas for biphenyl it corresponds to the decrease of the Pauli repulsion, that consequently reduces the steric contribution.

The interaction energy between $[Hg_3(o\text{-}C_6F_4)_3]$ and $\{Au_3(\mu\text{-}C(OEt)=NC_6H_4CH_3)_3\}$ (model **7**) showed that the stabilization of the complex is only attributed to the dispersion forces, mainly associated to the metallophilic interactions. Despite that the orbital and electrostatic contributions were very high compared to the models **1-6**, the Pauli repulsion was even higher. These results are supported by the energies obtained at the HF level, which show that without electronic correlation there is no attractive interaction between the fragments. The addition of a new layer of $\{Au_3(\mu\text{-}C(OEt)=NC_6H_4CH_3)_3\}$ to $[Hg_3(o\text{-}C_6F_4)_3]$ (model **8**) increased to the double all of the stabilizing energy contributions, while Pauli repulsion increases slightly more than double. Consequently, the interaction energy increased to a magnitude close to the double of the energy obtained for model with just one $\{Au_3(\mu\text{-}C(OEt)=NC_6H_4CH_3)_3\}$, revealing an extensive behavior of the interaction energy for these particular systems. However, the slight decrease of the interaction energy with two layers caused by the Pauli repulsion is expected to affect the extensive nature of the interaction energy with the increase of the number of layers.

C. Time-Dependent (TD) DFT calculations

For adducts **1-6**, the UV-visible spectra have been reported experimentally.[6-8] The electronic spectrum of the $[Hg_3(o\text{-}C_6F_4)_3]\{Au_3(\mu\text{-}C(OEt)=NC_6H_4CH_3)_3\}$ complex has not been published, so the results obtained here have a predictive character. We calculated the allowed spin singlet transition for this complex, based on the ground state structures

of models **1-8** at the TPSS-D3 level. Only singlet-singlet transitions were considered in these scalar quasirelativistic calculations. Here, we consider as allowed transitions those whose oscillator strength is different from zero. The allowed transitions and active molecular orbitals obtained are shown in Figures 3-6 and described in Tables 5 and 6.

$[Hg(C_6F_5)_2]$-{L} (1-3). The electronic structure of the models have been described with one absorption peak at 329, 272 and 305 nm for naphthalene, biphenyl, and fluorene, respectively. These theoretical results are very close to those reported experimentally (320, 290 and 300 nm)[8] for the same systems studied here.

For the three models the assigned to individual band of type ligand-to-metal-ligand charge transfer (LMLCT). The theoretical calculations are described in Table 5. The bands are an excitation of type $\pi^* \rightarrow d_{xy} + \pi^*$. We must point out that the orbital base corresponds to a π^* orbital of the arene molecule. Thus, the transition involved in this orbital goes to a mercury complex orbital (d_{xy}) and π^* centered above arene. The active molecular orbitals in the electronic transition are shown in Figure 3.

$[Hg_3(o\text{-}C_6F_4)_3]_2$-{L} (4-6). We observed a red shift of the excited bands of the same molecules of arenes as in models **1-3** above (see Table 5). All the models have been described with one absorption peak at 320, 335 and 342 nm for naphthalene, biphenyl, and fluorene, respectively. There is a good agreement with those reported experimentally (300, 295 and 320 nm).[8] The bands are mainly LMLCT, LMLCT and MLMCT for naphthalene, biphenyl, and fluorene, respectively (**4-6**). These transitions can be understood from the MOs shown in Figure 4. In general, the transitions involve the mercury-arene-to-mercury-arene orbitals.

$[Hg_3(o\text{-}C_6F_4)_3]\{Au_3(\mu\text{-}C(OEt)=NC_6H_4CH_3)_3\}n$ (7-8). The electronic spectrum of model **7** has been described with four absorption peaks at 400, 337, 299 and 279 nm assigned to individual states of a metal-ligand-to-metal-ligand, metal-ligand-to-ligand and ligand-to-ligand charge transfer (MLMLCT, MLLCT and LLCT). The theoretical calculations are described in Table 6. The bands are a mixture of excitations show in Figure 5. Most of the transitions involve $[Hg_3(o\text{-}C_6F_4)_3]$ and $\{Au_3(\mu\text{-}C(OEt)=NC_6H_4CH_3)_3\}$ fragments.

On the other hand**,** when we used model **8**, we saw a red shift of the excited bands at 438, 391, 354, 323 and 287 nm (see Table 5). The bands are mainly the same as those of model **7**, which can be understood from the MOs shown in Figure 6. The transition involves the metallophilic interaction between $[Hg_3(o\text{-}C_6F_4)_3]$ and $\{Au_3(\mu\text{-}C(OEt)=NC_6H_4CH_3)_3\}$. There are no published experimental results with which we can check out our results theoretical. Thus, the description made is a proposal.

IV. Conclusion

This study provides further information on the nature of the mercury-carbon(arene) intermolecular interaction in the $[Hg(C_6F_5)_2]_2$-{L} and $[Hg_3(o\text{-}C_6F_4)_3]_2\cdot${L} (L = naphthalene, biphenyl, fluorene) adducts and on their spectroscopic properties. Theoretical calculations at the MP2, SCS-MP2 and DFT-D3 levels are in agreement with experimental geometries and van der Waals interactions between mercury and arene (Hg-arene). We have found that the energy interaction is mainly due to an electronic correlation effect, with a high dispersive component. For the $[Hg_3(o\text{-}C_6F_4)_3]\{Au_3(\mu\text{-}C(OEt)=NC_6H_4CH_3)_3\}n$ (n = 1,2) complexes a strong metallophilic interaction was found between the mercury and gold fragments at the MP2, SCS-MP2 and DFT-D3 levels. For all the models studied, we found that at the SCS-MP2 method generates interaction

energies lower than MP2 and DFT-D3. On the other hand, our TD-DFT/TPSS-D3 calculations were able to predict the experimental excitation spectra of all adducts (**1-6**), thus validating our theoretical models. Finally, we presented a predictive spectra for adducts **7** and **8**.

Acknowledgements

This work has been funded by Fondecyt under projects 1100162, 1140503 and Project RC120001 of the Iniciativa Científica Milenio (ICM) del Ministerio de Economía, Fomento y Turismo del Gobierno de Chile. SMR thanks the financial support from Grant ICM No 120082. LBP thanks to Basal Financing Program CONICYT-FB0807 (CEDENNA) for their financial support.

References

1. M. Tsunoda and F.P. Gabbaï, *J. Am. Chem. Soc.*, 2000, **122**, 8335.

2. M.R. Haneline, M. Tsunoda and F.P. Gabbaï, *J. Am. Chem. Soc.*, 2002, **124**, 3737.

3. M.R. Haneline, R.E. Taylor and F.P. Gabbaï, *Chem. Eur. J.*, 2003, **9**, 5189.

4. M.R. Haneline, J.B. King and F.P. Gabbaï, *Dalton Trans.*, 2003, **45**, 2686.

5. C. Burress, O. Elbjeirami, M.A. Omary and F.P. Gabbaï, *J. Am. Chem. Soc.*, 2005, **127**, 12166.

6. T.J. Taylor and F.P. Gabbaï, *Organometallics*, 2006, **25**, 2143.

7. T.J. Taylor, C,N. Burress and F.P. Gabbaï, *Organometallics*, 2007, **26**, 5252.

8. C.N. Burress, M.I. Bodine, O. Elbjeirami, J.H. Reibenspies, M.A. Omary and F.P. Gabbäi, *Inorg. Chem.*, 2007, **46**, 1388.

9. O. Elbjeirami, C.N. Burress, F.P. Gabbaï and M.A. Omary, *J. Phys. Chem. C*, 2007, **111**, 9522.

10. T.J.Taylor, O. Elbjeirami, C.N. Burress, M. Tsunoda, M.I. Bodine, M.A. Omary and F.P. Gabbaï, *J. Inorg. Organomet. Polym.*, 2008, **18**, 175.

11. I.A. Tikhonova, D.A. Gribanyov, K.I. Tugashov, F.M. Dolgushin, A.S. Peregudov, D.Y. Antonov, Y.I. Rosenberg and V.B. Shur, *J. Organometallic Chem.*, 2010, **659**, 1949.

12. H. Chiniforoshan, N. Pourrahim, L. Tabrizi, H. Tavakol, M.R. Sabzalian and B. Notash, *Inorg. Chimi. Acta*, 2014, **416**, 85.

13. F.M. Dolgushin, A.F. Smol´yakov, K. Yu. Supoitsky, A.V. Vologzhanina, I.V. Fedyanin, S.V. Shishkina, *Struct. Chem.,* 2015 DOI 10.1007/s11224-015-0646-0

14. A. Burini, J.P. Fackler, R. Galassi, T.A. Grant, M.A. Omary, M.A. Rawashdeh-Omary, B.R. Pietroni and R.J. Staples, *J. Am. Chem. Soc.*, 2000, **122**, 11264.

15. A. Burini, J.P. Fackler, R. Galassi, A. Macchioni, M.A. Omary, M.A. Rawashdeh-Omary, B.R. Pietroni, A. Sabatini, and C. Zuccaccia, *J. Am. Chem. Soc* ., 2002, **124**, 4570.

16. F. Mendizabal, *Int. J. Quantum Chem.*, 1999, **73**, 317.

17. F. Mendizabal, *Organometallics*, 2001, **20**, 261.

18. F. Mendizabal, D. Burgos and C. Olea-Azar, *Chem. Phys. Lett*., 2008, **463**, 272.

19. J.-M. Lehn, *Chem. Soc. Rev*., 2007, **36**, 151.

20. H.-J. Scheider, *Angew. Chem. Int. Ed*., 2009, **48**, 3924.

21. J.-M. Lehn, *Rep. Prog. Phys.*, 2004, **64**, 249.

22. G. Chalasinski and M.M. Szczesniak, *Chem. Rev.* 2000, **100**, 4227.

23. D. Braga and F. Grepioni, *Acc. Chem. Res.* 2000, **33**, 601.

24. A.D. Buckingham, *Basic Theory of Intermolecular Forces: Applications to Small Molecules, in Intermolecular Interactions: From Diatomics to Biopolymers*, Ed. B. Pullman, Wiley, Chichester, pp. 1-67, 1978.

25. F.J.M. Hoeben, P. Jonkheijm, E.W. Meijer and A.P.H. Schennig, *Chem. Rev.* 2005, **105**, 1491.

26. A.J. Stone*, The Theory of Intermolecular Forces,* Clarendon Press, Oxford, 1996.

27. D. Braga and F. Grepioni, *Chem. Commun.* 2005, **41**, 3635.

28. E. Pensa, E. Cortés, G. Corthey, P. Carro, C. Vericat, M.H. Fonticelli, G. Benítez, A.A. Rubert and R.C. Salvarezza, *Acc. Chem. Res.,* 2012, **45**,1183.

29. P. Pyykkö, *Chem. Rev*., 1997, **97**, 597.

30. P. Pyykkö, *Angew. Chem. Int. Ed*., 2004, **43**, 4412.

31. P. Pyykko, N. Runemberg and F. Mendizabal, *Chem. Eur. J*., 1997, **3**, 1451.

32. P. Pyykkö and F. Mendizabal, *Inorg. Chem.*, 1998, **37**, 3018.

33. M.R. Haneline and F.P. Gabbaï, *Inorg. Chem*., 2005, **44**, 6248.

34. S. Grimme, J. Antony, S. Ehrlich and H. Krieg, *J. Chem. Phys.,* 2010, **132**, 154104.

35. W. Hujo and S. Grimme, *J. Chem. Theory. Comput.,* 2011, **7**, 3866.

36. S. Grimme, *ChemPhysChem*, 2012, **13**, 1407.

37. S. Grimme, *J. Chem. Phys.*, 2003, **118**, 9095.

38. M. Gernkamp, S. Grimme, *Chem. Phys. Letters*, 2004, **392**, 229.

39. P. Pyykkö, X.-G. Xiong, J. Li*, Faraday Discuss*., 2011,**152**, 169.

40. F. Mendizabal, S. Miranda-Rojas and L. Barrientos, *Comp. Theor. Chem.,* 2015, **1057,** 74.

41. M.E. Casida, C. Jamorski, K.C. Casida and D.R. Salahub, *J. Chem. Phys.,* 1998, **108**, 4439.

42. L. Olsen and P. Jϕrgensen, *In Modern Electronic Structure Theory*, Vol. 2, Ed. D.R. Yarkony, World Scientific: River Edge, NJ, 1995.

43. R. Ahlrichs, M. Bär, M. Häser, H. Horn and C. Kölmel, *Chem. Phys. Lett*., 1989, **162**, 165.

44. D. Andrae, U. Häusserman, M. Dolg, H. Stoll and H. Preuss, *Theor. Chim. Acta*, 1990, **77**, 123.

45. P. Pyykkö, M. Straka and T. Tamm, *Phys. Chem. Chem. Phys*., 1999, **1**, 3441.

46. K. Eichkorn, O. Treutler, H. Öhm, M. Häser and R. Ahlrichs, *Chem. Phys. Lett*., 1995, **240**, 283.

47. G. te Velde, F. M. Bickelhaupt, E. J. Baerends, C. Fonseca Guerra, S. J. A. van Gisbergen, J. G. Snijders and T. Ziegler, *J. Comput. Chem*., 2001, **22**, 931.

48. E. R. Johnson, S. Keinan, P. Mori-Sánchez, J. Contreras-García, A. J. Cohen and W. Yang, *J. Am. Chem. Soc*., 2010, **132**, 6498.

49. J. Contreras-García, E. R. Johnson, S. Keinan, R. Chaudret, J.-P. Piquemal, D. N. Beratan and W. Yang, *J. Chem. Theory Comp*., 2011**, 7**, 625.

50. J.M. López-de-Luzuriaga, M. Monge, M.E. Olmos, and D. Pascual and T. Lasana, *Chem. Commun.,* 2011, **47**, 6795.

51. J.M. López-de-Luzuriaga, M. Monge, M.E. Olmos and D. Pascual, *Inorg. Chem.,* 2014, **53**, 1275.

Scheme Captions

Scheme 1. $Hg(C_6F_5)_2]_2\cdot\{L\}$ and $[Hg_3(C_6F_4)_3]_2\cdot\{L\}$ (L = naphthalene, biphenyl and fluorene) models (**1-6**).

Scheme 2. $Hg_3(C_6F_4)_3]\cdot\{Au_3(\mu\text{-}C(OEt)=NC_6H_4CH_3)_3\}_n$ (n =1,2) models (**7,8**).

Figure Captions

Figure 1. Binding modes and NCI analysis of the $[Hg(C_6F_5)_2]_2$-{L}**,** L = naphthalene (A), fluorine (B), biphenyl (C). The isosurfaces (s=0.45 a.u.) are colored using a blue-green-red (BGR) color scale.

Figure 2. Binding modes and NCI analysis of the $[Hg_3(C_6F_4)_3]_2\cdot\{L\}$, L = naphthalene (A), biphenyl (B) and fluorine (C). The isosurfaces (s=0.45 a.u.) are colored using a blue-green-red (BGR) color scale.

Figure 3. Active molecular orbitals in the electronic transitions of $Hg(C_6F_5)_2]_2\cdot\{$naphthalene$\}$ **(1)**, $[Hg(C_6F_5)_2]_2\cdot\{$biphenyl$\}$ **(2)** and $[Hg(C_6F_5)_2]_2\cdot\{$fluorene$\}$ **(3)** at the TPSS-D3 level.

Figure 4. Active molecular orbitals in the electronic transitions of $[Hg_3(C_6F_4)_3]_2\cdot\{$naphthalene$\}$ **(4),** $[Hg_3(C_6F_4)_3]_2\cdot\{$biphenyl$\}$ **(5)** and $[Hg_3(C_6F_4)_3]_2\cdot\{$fluorene$\}$ **(6)** at the TPSS-D3 level.

Figure 5. Active molecular orbitals in the electronic transitions of $[Hg_3(C_6F_4)_3]\cdot\{Au_3(\mu\text{-}C(OEt)=NC_6H_4CH_3)_3\}$ (**7**) at the TPSS-D3 level.

Figure 6. Active molecular orbitals in the electronic transitions of $[Hg_3(C_6F_4)_3]_2\cdot\{Au_3(\mu\text{-}C(OEt)=NC_6H_4CH_3)_3\}_2$ (**8**) at the TPSS-D3 level.

Table 1. Main geometric parameters of the $[Hg(C_6F_5)_2]_2$·{L} (L = naphthalene, biphenyl and fluorene) complexes (distances in pm and angles in degrees). Equilibrium geometry complex energies, $V(R_e)$ (kJ/mol), between $[Hg(C_6F_5)_2]_2$ and {L} with counterpoise (CP) correction.

System	Method	HgC[a]	HgC[b]	CF	CHgC[o]	$V(R_e)$
$[Hg(C_6F_5)_2]_2$·{naphthalene} (**1**)	HF	209.2	359.1	131.3	177.5°	-29.9
	MP2	209.2	339.5	131.3	177.5°	-214.4
	SCS-MP2	209.4	340.1	131.3	177.6°	-122.5
	PBE	209.2	344.1	131.5	177.5°	-15.7
	PBE-D3	209.2	341.6	131.3	177.5°	-105.7
	TPSS	210.1	396.7	131.4	178.5°	-4.3
	TPSS-D3	208.9	344.6	131.5	179.2°	-98.1
	B97	210.4	402.1	130.7	178.4°	-3.8
	B97-D3	210.3	374.9	130.5	178.5°	-70.9
$[Hg(C_6F_5)_2]_2$·{biphenyl} (**2**)	HF	208.9	390.5	131.2	179.2°	-34.1
	MP2	208.9	347.8	131.3	179.3°	-213.4
	SCS-MP2	209.1	348.5	131.2	179.2°	-111.2
	PBE	208.8	364.1	131.3	179.3°	-23.7
	PBE-D3	208.9	357.4	131.3	179.3°	-117.2
	TPSS	209.3	371.9	131.5	178.8°	-8.6
	TPSS-D3	209.9	347.7	131.6	177.6°	-130.2
	B97	210.3	432.5	130.7	179.4°	-7.9
	B97-D3	210.8	349.7	130.8	177.5°	-74.6
$[Hg(C_6F_5)_2]_2$·{fluorene} (**3**) (C_1)	HF	209.1	385.1	131.2	179.5°	-50.5
	MP2	209.0	350.8	131.3	178.1°	-251.7
	SCS-MP2	209.3	252.6	131.2	178.2°	-125.4
	PBE	209.0	369.4	131.4	178.1°	-24.8
	PBE-D3	209.1	360.9	131.4	178.2°	-130.8
	TPSS	209.1	369.6	131.3	178.2°	-8.3
	TPSS-D3	209.0	362.3	131.4	178.2°	-149.3
	B97	209.1	418.7	131.4	178.1°	-8.1
	B97-D3	209.1	360.1	131.4	178.2°	-145.4
$[Hg(C_6F_5)_2]$·{naphthalene}	Exp. [6-8]	205.7	332.3	134.7	178.5°	
$[Hg(C_6F_5)_2]$·{biphenyl}	Exp. [6-8]	206.8	351.0	134.5	179.2°	
$[Hg(C_6F_5)_2]$·{fluorene}	Exp. [6-8]	206.2	356.0	135.4	179.0°	

[a]Hg—C distance -C_6F_5 groups.
[b]Hg—C distance L.

Table 2. Main geometric parameters of $[Hg_3(C_6F_4)_3]_2$·{L} (L = naphthalene, biphenyl and fluorene) complexes (distances in pm and angles in degrees). Equilibrium geometry complex energies, $V(R_e)$ (kJ/mol), between $[Hg_3(C_6F_4)_3]_2$ and {L} with counterpoise (CP) correction.

System	Method	Hg-Hg[a]	HgC[b]	HgC[c]	CF	HgHgHg°	$V(R_e)$
$[Hg_3(C_6F_4)_3]_2$·{naphthalene} (**4**)	HF	367.0	210.3	336.1	131.5	60.0°	6.5
	MP2	366.9	210.3	310.3	131.5	60.0°	-115.1
	SCS-MP2	368.0	210.6	324.2	131.3°	60.0°	-98.4
	PBE	366.9	210.3	330.2	131.5	60.0°	-20.3
	PBE-D3	366.9	210.3	326.1	131.5	60.0°	-122.1
	TPSS	367.0	210.6	340.5	131.5	60.0°	-7.6
	TPSS-D3	367.1	210.5	323.3	131.8	60.0°	-156.4
	B97	369.5	212.1	402.5	131.3	60.0°	-6.9
	B97-D3	369.4	212.1	362.1	131.3	60.0°	-98.4
$[Hg_3(C_6F_4)_3]_2$·{biphenyl} (**5**)	HF	366.7	210.3	346.2	131.5	60.0°	-1.2
	MP2	366.8	210.3	312.5	131.5	60.0°	-110.5
	SCS-MP2	368.5	210.6	323.6	131.4°	60.0°	-96.5
	PBE	366.8	210.3	346.9	131.6	60.0°	0.7
	PBE-D3	366.6	210.3	326.2	131.6	60.0°	-139.1
	TPSS	367.3	210.5	342.5	131.8	60.0°	-6.1
	TPSS-D3	367.1	210.5	325.3	131.8	60.0°	-153.4
	B97	369.5	212.1	406.4	131.1	60.0°	-8.3
	B97-D3	369.5	212.1	358.9	131.2	60.0°	-116.8
$[Hg_3(C_6F_4)_3]_2$·{fluorene} (**6**)	HF	366.9	210.3	338.1	131.5	60.0°	11.0
	MP2	366.7	210.3	324.8	131.5	60.0°	-143.8
	SCS-MP2	368.1	210.5	325.2	131.4°	60.0°	-132.1
	PBE	366.9	210.3	338.1	131.5	60.0°	-24.4
	PBE-D3	366.7	210.3	326.1	131.5	60.0°	-154.2
	TPSS	367.1	210.6	341.4	131.8	60.0°	-6.9
	TPSS-D3	367.1	210.5	321.3	131.8	60.0°	-168.0
	B97	369.6	212.1	389.6	131.4	60.0°	-8.3
	B97-D3	369.7	212.1	314.8	131.4	60.0°	-127.2
$[Hg_3(C_6F_4)_3]$·{naphthalene}	Exp. [8]	360.8	207.4	340.3	135.2	60.0°	
$[Hg_3(C_6F_4)_3]$·{biphenyl}	Exp. [8]	361.0	206.9	342.2	136.2	60.0°	
$[Hg_3(C_6F_4)_3]$·{fluorene}	Exp. [8]	360.9	207.8	335.0	135.8	60.0°	

[a]Hg—Hg intramolecular distance.
[b]Hg—C distance -C_6F_4 groups.
[c]Hg—C distance L.

Table 3. Main geometric parameters of the $[Hg_3(C_6F_4)_3]\cdot\{Au_3(\mu\text{-}C(OEt)=NC_6H_4CH_3)_3\}_n$ (n =1,2) complexes (distances in pm and angles in degrees). Equilibrium geometry complex energies, $V(R_e)$ (kJ/mol), between $[Hg_3(C_6F_4)_3]_n$ and {L} with counterpoise (CP) correction.

System	Method	Au-Hg	Hg-Hg[a]	Au-Au[b]	Hg-C	Au-C	Au-N	V(R_e)
$[Hg_3(C_6F_4)_3]\cdot\{Au_3(\mu\text{-}C(OEt)=NC_6H_4CH_3)_3\}$ (**7**)	HF	396.3	374.1	333.9	212.2	201.7	211.8	-8.4
	MP2	329.5	365.6	331.2	212.1	201.5	211.7	-265.5
	SCS-MP2	331.6	366.4	331.5	212.2	201.5	211.7	-118.2
	PBE	362.5	366.4	333.9	211.5	201.5	211.8	-26.6
	PBE-D3	336.9	364.9	332.4	210.4	201.9	212.3	-200.4
	TPSS	347.0	365.5	331.9	210.6	202.3	211.9	-17.2
	TPSS-D3	327.6	364.3	331.7	210.8	202.5	211.9	-251.4
$[Hg_3(C_6F_4)_3]_2\cdot\{Au_3(\mu\text{-}C(OEt)=NC_6H_4CH_3)_3\}_2$ (**8**)	HF	406.9	372.6	343.5	212.0	208.0	214.3	-15.9
	MP2	325.4	365.5	332.1	212.1	201.6	210.5	-456.3
	SCS-MP2	330.5	366.5	331.5	212.2	201.5	211.5	-175.8
	PBE	363.5	363.5	363.9	341.7	210.1	201.7	-13.9
	PBE-D3	337.9	362.2	332.4	210.3	201.4	212.5	-381.0
	TPSS	347.2	363.4	331.6	210.5	201.8	212.3	-22.7
	TPSS-D3	328.5	361.0	331.1	210.3	201.5	212.1	-446.3
$[Hg_3(C_6F_4)_3]\cdot\{Au_3(\mu\text{-}C(OEt)=NC_6H_4CH_3)_3\}$	Exp. [14]	328.0 350.6	360.9	326.9	207.3	197.3	205.8	

[a]Hg—Hg intramolecular distance.
[a]Au—Au intramolecular distance.

Table 4. EDA Results for models 1-8. All the contributions to the interaction energy are in kJ/mol.

System	ΔE_{int} [a]	ΔE_{orb} [b]	ΔE_{elstat} [b]	ΔE_{pauli}	ΔE_{disp} [b]	ΔE_{int}* [c]
$[Hg(C_6F_5)_2]_2$·{naphthalene} (**1**)	-83.5	-31.6 (17.4%)	-51.7 (28.4%)	98.2	-98.4 (54.2%)	-82,9
$[Hg(C_6F_5)_2]_2$·{biphenyl} (**2**)	-104.1	-78.4 (18.8%)	-164.1 (39.5%)	311.8	-173.4 (41.7%)	-102.5
$[Hg(C_6F_5)_2]_2$·{fluorene} (**3**)	-123.1	-45.2 (15.9%)	-95.2 (33.6%)	160.4	-143.1 (50.5%)	-118.7
$[Hg_3(C_6F_4)_3]_2$·{naphthalene} (**4**)	-128.2	-42.1 (16.8%)	-74.5 (29.7%)	122.3	-133.9 (53.5%)	-126.8
$[Hg_3(C_6F_4)_3]_2$·{biphenyl} (**5**)	-148.0	-46.7 (17.4%)	-67.7 (25.3%)	120.1	-153.7 (57.3%)	-145.9
$[Hg_3(C_6F_4)_3]_2$·{fluorene} (**6**)	-161.3	-52.8 (16.9%)	-86.1 (27.5%)	151.3	-173.7 (55.6%)	-160.7
$[Hg_3(C_6F_4)_3]$·$\{Au_3(\mu\text{-}C(OEt)=NC_6H_4CH_3)_3\}$ (**7**)	-239.0	-136.1 (21.4%)	-232.1 (36.5%)	396.7	-267.5 (42.1%)	-231.4
$[Hg_3(C_6F_4)_3]_2$·$\{Au_3(\mu\text{-}C(OEt)=NC_6H_4CH_3)_3\}_2$ (**8**)	-456.0	-268.7 (21.0%)	-468.2 (36.6%)	824.1	-543.2 (42.4%)	-442.3

[a]Interaction energies calculated with ADF using the fragments at the complex geometry.
[b]Values in parentheses give the percentage contribution to the total attractive interactions ($\Delta E_{orb} + \Delta E_{elstat} + \Delta E_{disp}$).
[c]Interaction energies calculated with Turbomole (TPSS-D3) with the fragments at the complex geometry.

Table 5. TD-DFT/TPSS-D3 singlet-excitation calculations for $[Hg(C_6F_5)_2]_2 \cdot \{L\}$ and $[Hg_3(C_6F_4)_3]_2 \cdot \{L\}$ (L = naphthalene, biphenyl and fluorene).

System	λ_{calc}/nm	f^a	λ_{exp}/nm	Contributions[b]	Transition type
$[Hg(C_6F_5)_2]_2 \cdot \{naphthalene\}$ **(1)**	329	0.0642	320	162a → 164a (95)	LMLCT ($\pi^* \rightarrow d_{xy}+\pi^*$)
$[Hg(C_6F_5)_2]_2 \cdot \{biphenyl\}$ **(2)**	272	0.0650	290	158a → 169a (86)	LMLCT ($\pi^* \rightarrow d_{xy}+\pi^*$)
$[Hg(C_6F_5)_2]_2 \cdot \{fluorene\}$ **(3)**	305	0.0746	300	169a → 170a (82)	LMLCT ($\pi^* \rightarrow d_{xy}+\pi^*$)
$[Hg_3(C_6F_4)_3]_2 \cdot \{naphthalene\}$ **(4)**	320	0.0351	300	227a → 241a (76)	LMLCT ($d_{xy}+\pi^* \rightarrow d_{xy}+\pi^*$)
$[Hg_3(C_6F_4)_3]_2 \cdot \{biphenyl\}$ **(5)**	335	0.0221	295	244a → 246a (69)	LMLCT ($\pi^* \rightarrow d_{xy}+\pi$)
$[Hg_3(C_6F_4)_3]_2 \cdot \{fluorene\}$ **(6)**	342	0.0944	320	244a → 248a (75)	MLMCT ($dz^2+\pi^* \rightarrow \pi^*+ dz^2$)

[a]Oscillator strength.
[b]Values are $|coeff.|^2 \times 100$.

Table 6. TD-DFT/TPSS-D3 singlet-excitation calculations for $[Hg_3(C_6F_4)_3]_n \cdot \{Au_3(\mu\text{-}C(OEt)=NC_6H_4CH_3)_3$

Complexes	λ_{calc}	f^a	Contributions[b]	Transition type
$[Hg_3(C_6F_4)_3]\cdot\{Au_3(\mu\text{-}C(OEt)=NC_6H_4CH_3)_3\}$ (**7**)	400 (**A**)	0.0170	222a → 226a (70%)	MLMLCT (*dz2*+π*→*dz2*+π*)
	337 (**B**)	0.0202	222a → 229a (75%)	MLLCT (*dz2*+π*→π*)
	299 (**C**)	0.0314	218a → 227a (81%)	LLCT (π*→π*)
	279 (**D**)	0.0386	220a → 229a (75%)	MLMLCT (*dz2*+π*→*dz2*+π*)
$[Hg_3(C_6F_4)_3]\cdot\{Au_3(\mu\text{-}C(OEt)=NC_6H_4CH_3)_3\}_2$ (**8**)	438 (**A**)	0.0015	335a → 337a (97%)	MMLCT (6s+π*→ dz2+π*)
	391 (**B**)	0.0200	333a → 338a (78%)	MMLCT (dz2+π*→ dz2+π*)
	354 (**C**)	0.0250	331a → 338a (76%)	MMLCT (dz2+π*→ dz2+π*)
	323 (**D**)	0.0260	323a → 337a (75%)	LMLCT (π*→dz2+π*)
	287 (**E**)	0.0383	305a → 337a (55%)	MMLCT (d+π*→ dz2+π*)

[a]Oscillator strength.
[b]Values are $|\text{coeff.}|^2 \times 100$.

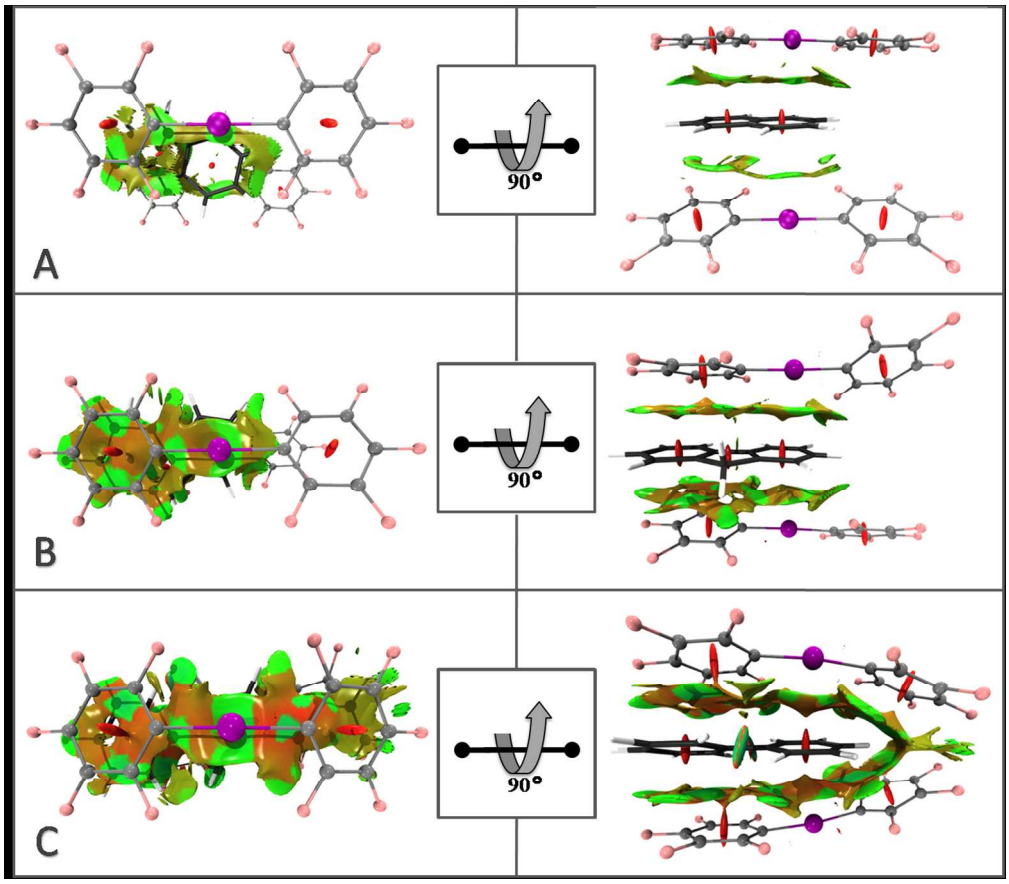

253x220mm (150 x 150 DPI)

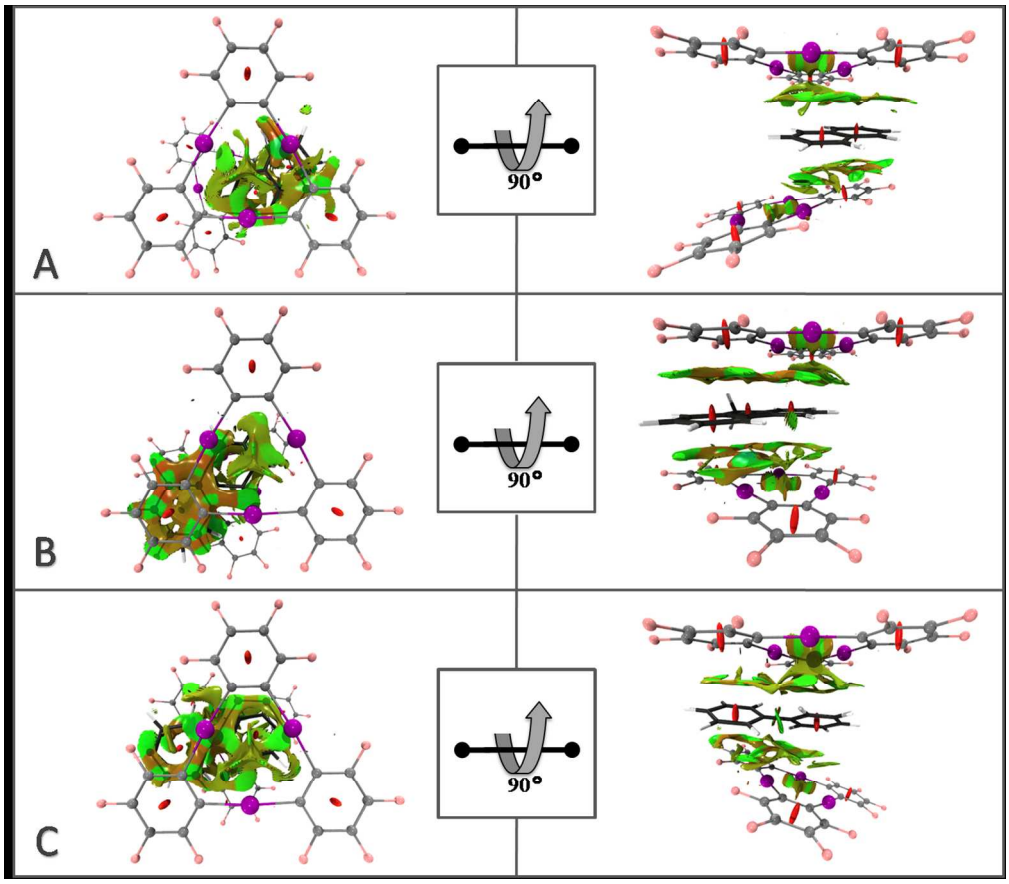

253x220mm (150 x 150 DPI)

$[Hg(C_6F_5)_2]_2$·{naphthalene} (1)

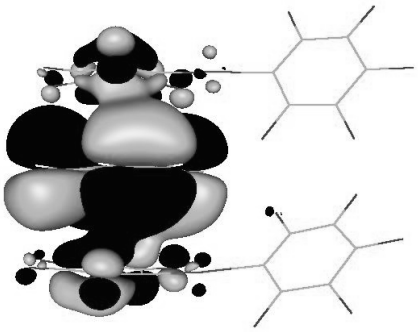

162a (HOMO)

329 nm

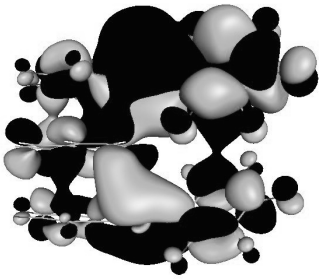

164a (LUMO+1)

$[Hg(C_6F_5)_2]_2$·{biphenyl} (2)

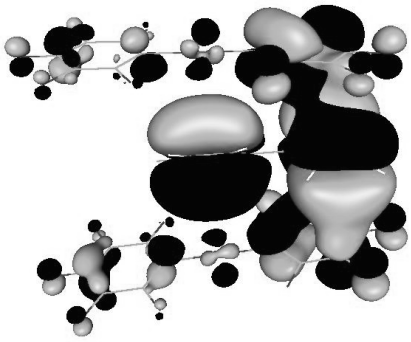

158a (HOMO-9)

272 nm

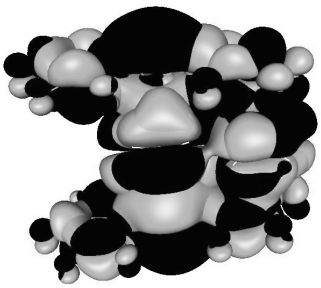

169a (LUMO+2)

$[Hg(C_6F_5)_2]_2$·{fluorene} (3)

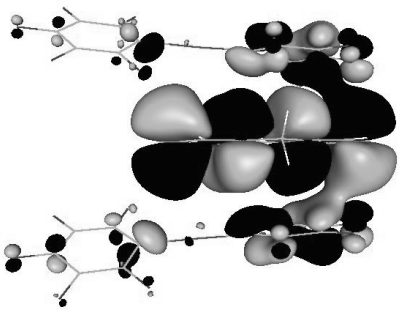

169a (HOMO)

305 nm

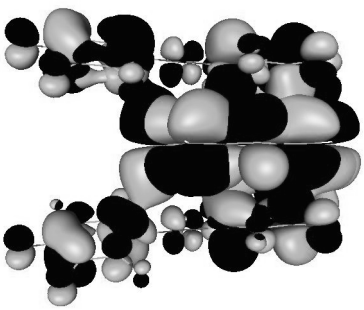

170a (LUMO)

Figure 3

$[Hg_3(C_6F_4)_3]_2$·{naphthalene} (4)

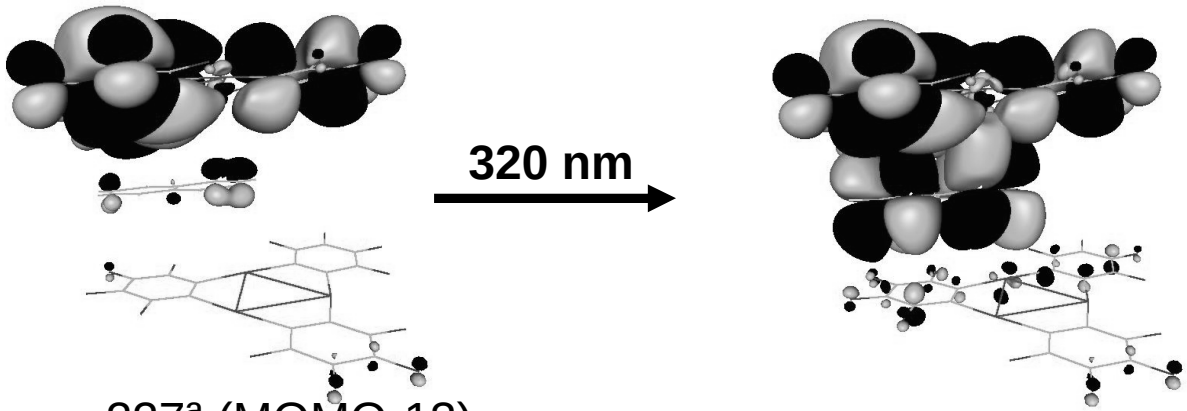

227[a] (MOMO-13) 241[a] (LUMO)

$[Hg_3(C_6F_4)_3]_2$·{biphenyl} (5)

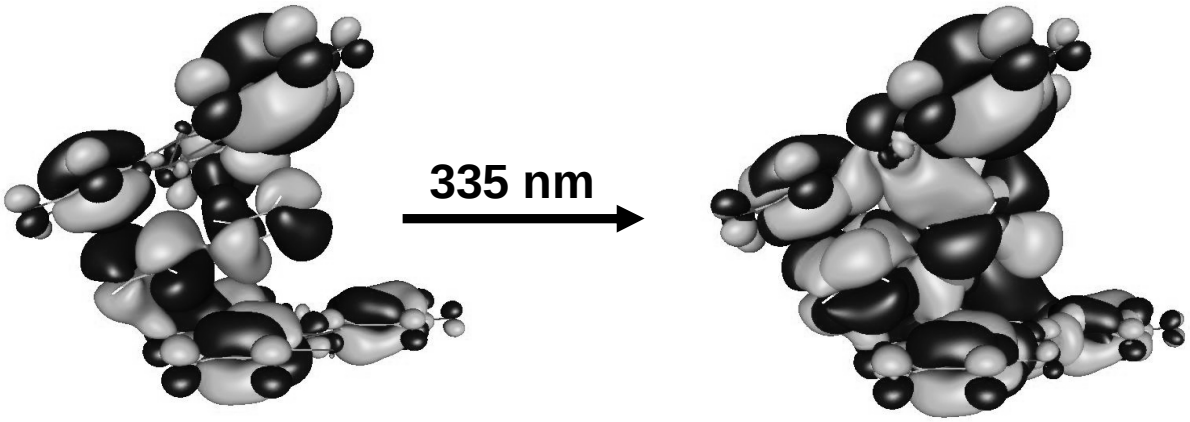

244a (HOMO-1) 246a (LUMO)

$[Hg_3(C_6F_4)_3]_2$·{fluorene} (6)

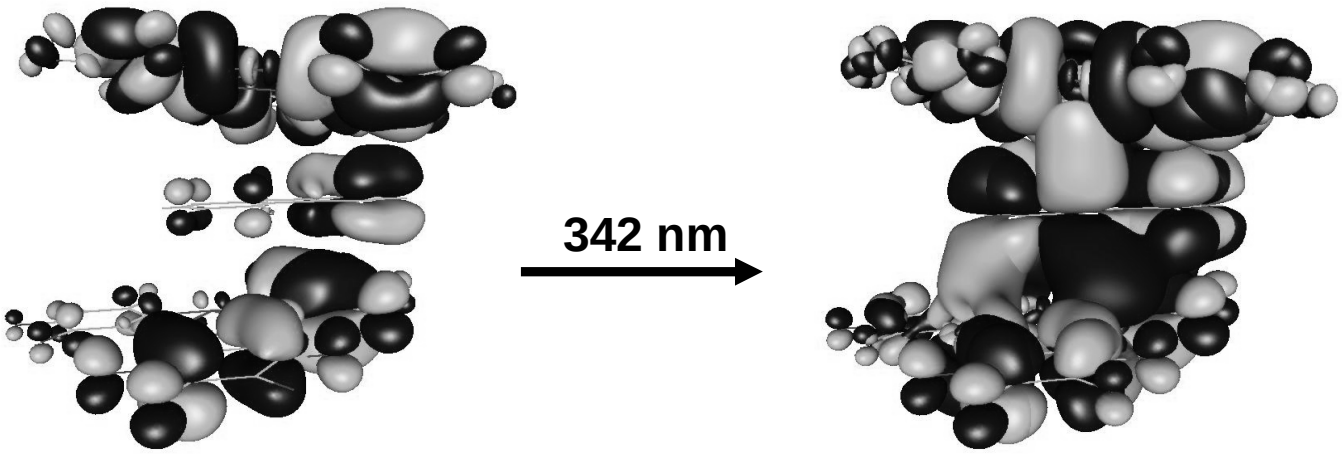

244a (HOMO-3) 248a (LUMO)

Figure 4

$[Hg_3(C_6F_4)_3]\cdot\{Au_3(\mu\text{-}C(OEt)=NC_6H_4CH_3)_3\}$ (7)

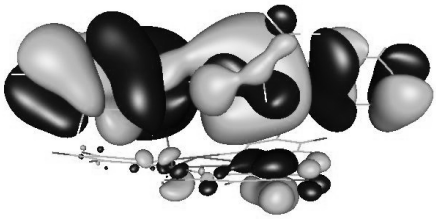

222a (HOMO)

400 nm (A)

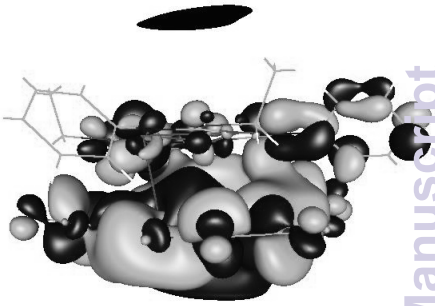

226a (LUMO+4)

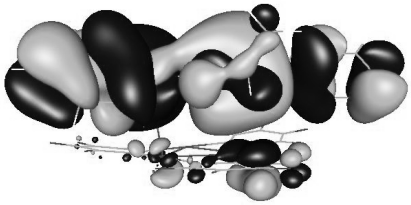

222a (HOMO)

337 nm (B)

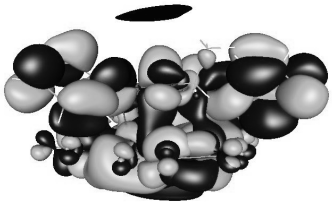

229a (LUMO+7)

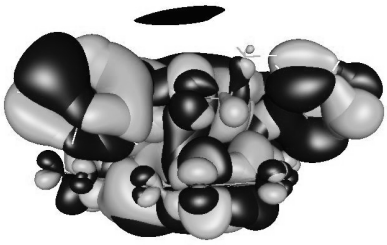

218a (HOMO-4)

299 nm (C)

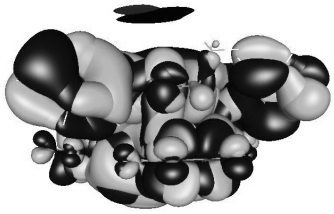

227a (LUMO+5)

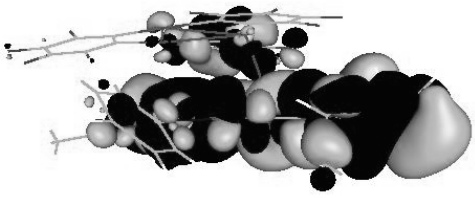

220a (HOMO-2)

279 nm (D)

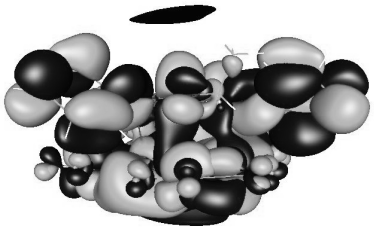

229a (LUMO+7)

Figure 5

$[Hg_3(C_6F_4)_3]_2 \cdot \{Au_3(\mu\text{-}C(OEt)=NC_6H_4CH_3)_3\}_2$ (8)

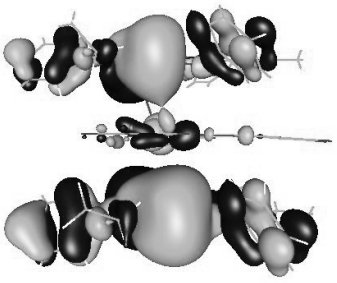

335a (HOMO-1)

438 nm (A)

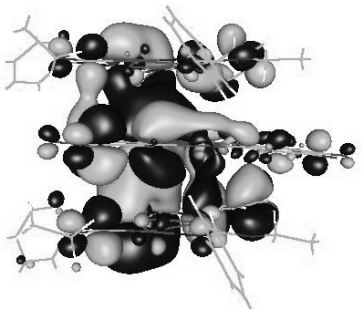

337a (LUMO)

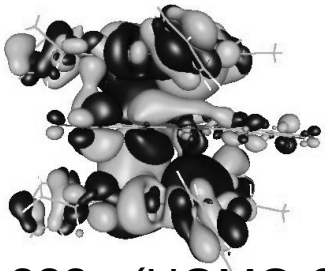

333a (HOMO-3)

391 nm (B)

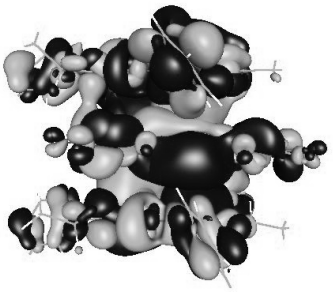

338a (LUMO+1)

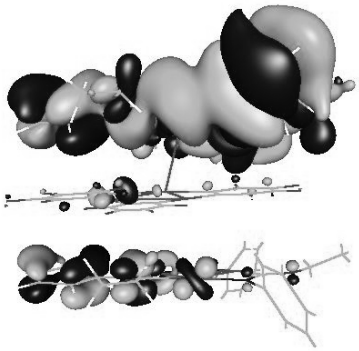

331a (HOMO-5)

354 nm (C)

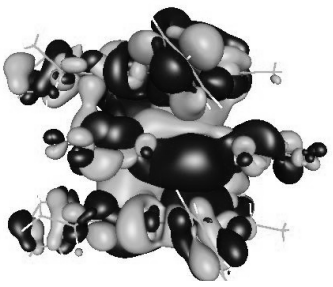

338a (LUMO+1)

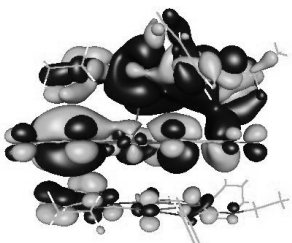

323a (HOMO-13)

323 nm (D)

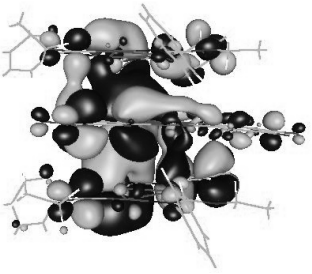

337[a] (LUMO)

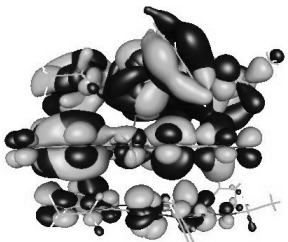

305a (HOMO-30)

287 nm (E)

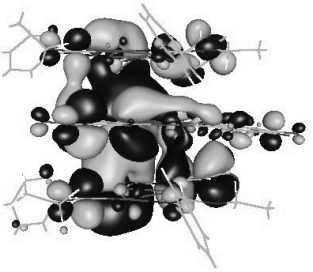

337a (LUMO)

Figure 6

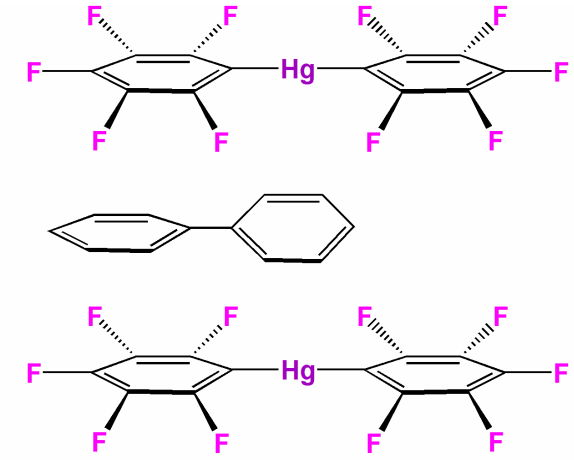

1

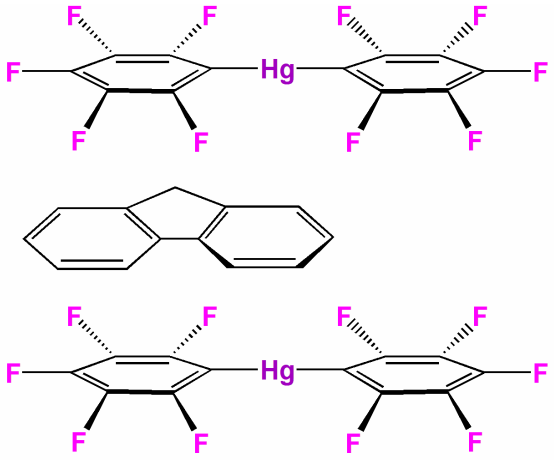

2

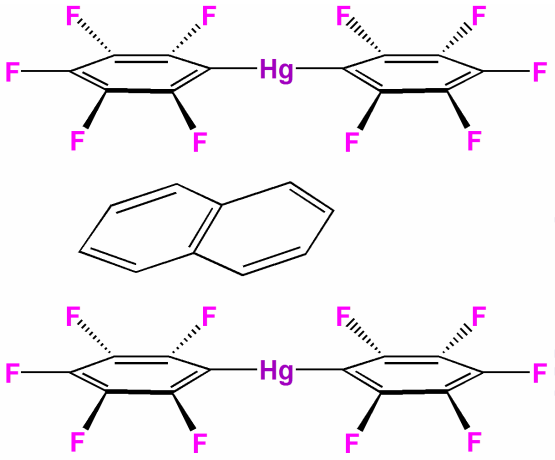

3

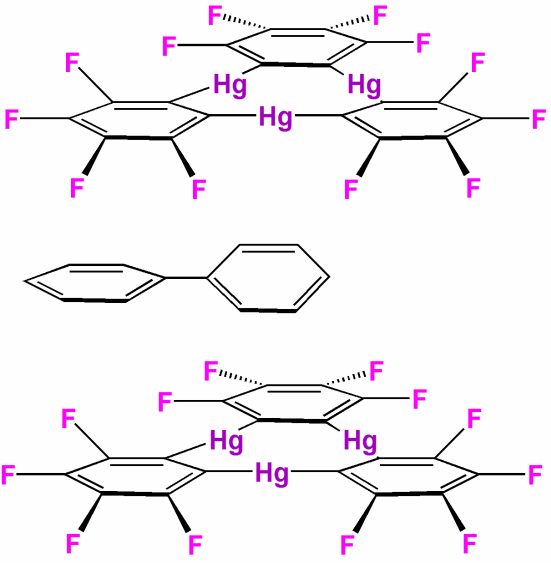

4

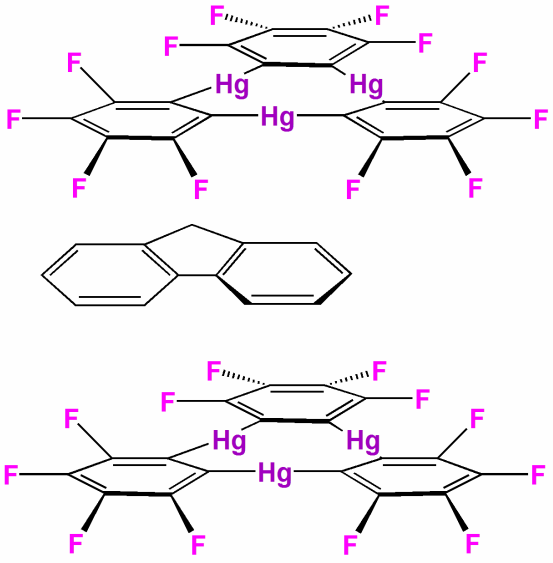

5

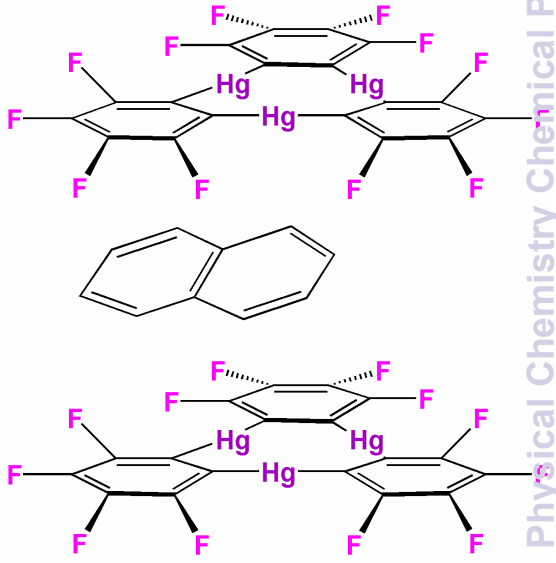

6

Scheme 1

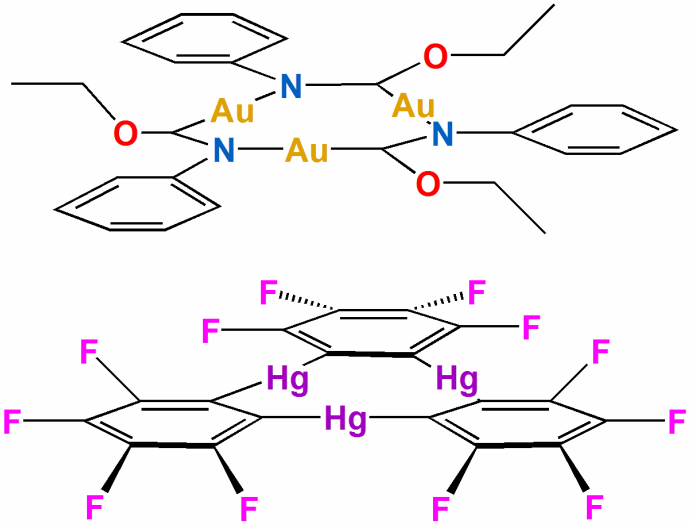

7

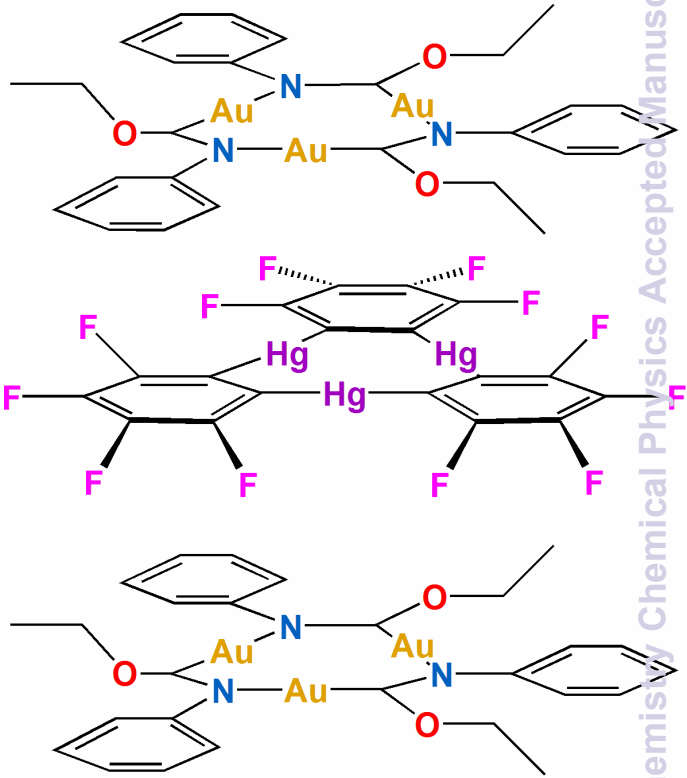

8

Scheme 2